American Journal of Materials Research
2014; 1(1): 7-13
Published online March 20, 2014 (http://www.aascit.org/journal/ajmr)

Keywords
$LiTaSiO_5$,
Nano Scale,
Grain Size,
Band Gap Energy,
Semiconductor

Received: December 11, 2013
Revised: March 11, 2014
Accepted: March 12, 2014

Effect of annealing times for $LiTaSiO_5$ thin films on structure, nano scale grain size and band gap

Irzaman[1], Irmansyah[1], Heriyanto Syafutra[1], Ardian Arif[1], Husin Alatas[1], Yuli Astuti[1], Nurullaeli[1], Ridwan Siskandar[1], Aminullah[1], Gusti Putu Agus Sumiarna[1], Zul Azhar Zahid Jamal[2]

[1]Department of Physics, Faculty of Mathematics and Natural Sciences, Bogor Agricultural University, Bogor, Indonesia
[2]School of Microelectronic Engineering, Universiti Malaysia Perlis, Malaysia

Email address
irzamanhusein@yahoo.com (Irzaman)

Citation
Irzaman, Irmansyah, Heriyanto Syafutra, Ardian Arif, Husin Alatas, Yuli Astuti, Nurullaeli, Ridwan Siskandar, Aminullah, Gusti Putu Agus Sumiarna, Zul Azhar Zahid Jamal. Effect of Annealing Times for $LiTaSiO_5$ Thin Films on Structure, Nano Scale Grain Size and Band Gap. *American Journal of Materials Research.* Vol. 1, No. 1, 2014, pp. 7-13

Abstract
This research was focused on structure, nano scale grain size, and band gap of $LiTaSiO_5$. $LiTaSiO_5$ thin films were manufactured by using chemical solution deposition (CSD) at annealing temperature of 800 ^oC for 1, 8, 15, and 22 hours, then reacted with *p*-type Si (100) substrates. The X-Ray Diffraction (XRD) results at 800 ^oC for 1, 8, 15, and 22 hours showed phase transformation from $LiTaO_3$ into $LiTaSiO_5$. The XRD and Atomic Force Microscopy (AFM) analysis were utilized for calculating nano scale grain size. The AFM can show more detail data than the XRD. The band gap energy which was resulted from Tauc plot, showed that $LiTaSiO_5$ thin films belong to semiconductor materials.

1. Introduction

Lithium Tantalate ($LiTaO_3$) and Lithium Tantalum Silicate ($LiTaSiO_5$) are attractive materials for nonlinear and integrated optics [1,2]. They are well known multifunctional material, widely used in the fields of piezoelectric, ferroelectric, acoustooptic, electrooptic and nonlinear optic devices [3]. $LiTaO_3$ and $LiTaSiO_5$ are materials with high sensitivity to heat. $LiTaO_3$ is a ferroelectric crystal which undergo high Curie temperature of 608 ^oC and has high melting point of 1650 ^oC [4].

$LiTaO_3$ and $LiTaSiO_5$ can be manufactured by various methods, such as chemical solution deposition (CSD) [5-8], metal organic chemical vapor deposition (MOCVD) [9,10], rf sputtering [11,12] and Pulsed Laser Ablation Deposition (PLAD) [13]. In this research, thin film is manufactured by CSD with reacting lithium acetate, tantalum oxide, 2.5 ml 2-methoxyethanol solvent 1.0 M and SiO_2 at temperature of 600 ^oC. Advantages of CSD process are good quality, easy procedure, low cost and can be produced at room temperature [14].

$LiTaSiO_5$ thin films can be applicated as a infrared sensor due to their frequencies are in the infrared region where $LiTaSiO_5$ in this region can be vibrated, bending

and stretching. The nanoscale surface roughness and grain size of the thin films were analyzed by using AFM. Instead of tunneling current, the AFM detects interatomic forces that occur between a cantilever probe tip and sample. Normal imaging forces in the range of 1 - 50 nano Newton and cantilever deflections of less than 0.1 nm can be detected (nano scale) [15,16].

2. Methods

$LiTaSiO_5$ thin films were manufactured by CSD at annealing temperature of 800 ^oC for 1, 8, 15, and 22 hours, then reacted with *p*-type Si (100) substrates using lithium acetate, tantalum oxide, and 2.5 ml 2-methoxyethanol solvent 1.0 M inside Ultrasonic chamber for 2 hours which produced a clear liquid. After 20 minutes at room temperature, this solution was spin coated on *p*-type Si (100) substrates of 10 mm x 10 mm at a speed of 3000 rpm for 30 seconds.

Annealing process was conducted in a Furnace Model Nabertherm Type 27. The nano scale surface roughness and grain size of thin films, which were described by AFM Model SPA 300 (Seiko Instruments Industry, Co., Japan) on 2000 nm x 2000 nm area at room temperature, were conducted in School of Microelectronic Engineering, Universiti Malaysia Perlis, Jalan Bukit Lagi, 01000 Kangar Perlis, Malaysia. This analysis was conducted for measuring surface topography.

In addition, Shimadzu XRD-7000 of 2θ range from 10^o to 80^o with step of 0.02^o was used in this research for identifying crystallite structure of $LiTaSiO_5$.

For calculating crystallite size, Scherres equation was used in this research which has derived an expression for broadening of x-ray diffraction peaks due only to small crystallite sizes :

$$B_{crystallite} = \frac{k\lambda}{L\cos\theta} \quad (1)$$

Where λ is the wavelength of x-ray used, θ is the Bragg angle, L is the "average" crystallite size measured in a direction perpendicular to the surface of the specimen, and k is a constant. However this equations is now frequency used to estimate the crystallite size of both cubic and non cubic materials. The constant k in equation (4) has been determined to vary between 0.89 and 1.39, but is usually taken at close to unity. Since the precision of crystallite-size analysis by this method is, at best, about ±10%, the assumption that k = 1.0 is generally justifiable.

In the observed x-ray has a width B_0, and the width do to instrumental effects is B_i, then the remaining width B_r is due to the combined effect of crystallite size and lattice strain :

$$B_r = B_0 - B_i \quad (2)$$

This expression is true only when the peak has a Lorentzian (Cauchy) profile. However, if it has a Gaussian profile, better expression is

$$B_r^2 = B_0^2 - B_i^2 \quad (3)$$

In the absence of clear-cut evidence for the exact nature of the peak, the geometric mean was used to get a more nearly correct expression :

$$B_0 = \sqrt{(B_0 - B_i)\sqrt{B_0^2 - B_i^2}} \quad (4)$$

In the analysis, however, equation (2) was used to subtract the instrumental broadening from the observed broadening.

The lattice strain in the material also causes broadening of the diffraction peaks, which can be represented by the relationship

$$B_{strain} = \eta \tan\theta \quad (5)$$

where η is the strin in the material.

The width, B_r, of the diffraction peak after subtracting the instrumental effect can now be considered as the sum of widths due to small crystallite sizes and lattice strains :

$$B_r = B_{crystallite} + B_{strain} \quad (6)$$

and from equations (4) and (5)

$$B_r = \frac{k\lambda}{L\cos\theta} + \eta\tan\theta \quad (7)$$

Multiplying equation (7) by $\cos\theta$

$$B_r \tan\theta = \frac{k\lambda}{L} + \eta\sin\theta \quad (8)$$

Thus, it was clear that when $B_r \cos\theta$ was plotted against $\sin\theta$, a straight line was obtained with slope η and intercepts $k\lambda/L$, the crystallite size L can be calculated from the intercept by using the appropriate values of k (generally taken to be = 1.0) and λ [18].

According to the Bragg law of diffraction:

$$2d\sin\theta = n\lambda \quad (9)$$

Where d is plane distance, θ is diffraction angle and λ is wavelength (Cu = 1.50546 Å).

Lattice parameters, which were found by Cohen method, were eliminated by choosing right extrapolation function and random errors which were reduced by least quadratic method so that it can be very accurate[24].

To find monoclinic lattice parameter with several peaks, the plane distance,d[24].

$$\frac{1}{d^2} = \frac{1}{\sin^2\beta}\left(\frac{h^2}{a^2} + \frac{k^2\sin^2\beta}{b^2} + \frac{l^2}{c^2} - \frac{2hlcos\beta}{ac}\right) \quad (10)$$

Lattice parameter values are given by:

$$\sin^2\theta = \frac{\lambda^2}{4}\left[\frac{1}{\sin^2\beta}\left(\frac{h^2}{a^2} + \frac{k^2\sin^2\beta}{b^2} + \frac{l^2}{c^2} - \frac{2hlcos\beta}{ac}\right)\right] \quad (11)$$

and

$$\sin^2\theta - \frac{\lambda^2}{4a^2}\left(\frac{h^2}{\sin^2\beta}\right) + \frac{\lambda^2}{4b^2}(k^2) + \frac{\lambda^2}{4c^2}\left(\frac{l^2}{\sin^2\beta}\right) - \frac{\lambda^2}{2ac}\left(\frac{hlcos\beta}{\sin^2\beta}\right) = D\sin^2 2\theta$$

From those equations

$$\sin^2\theta = E\alpha + D\gamma + C\delta + B\varphi + A\tau,$$

Where

$$E = \frac{\lambda^2}{4a^2}, \quad \alpha = \frac{h^2}{\sin^2\beta}, \quad D = \frac{\lambda^2}{4b^2}, \quad \gamma = k^2, \quad C = \frac{\lambda^2}{4c^2},$$

$$\delta = \frac{l^2}{\sin^2\beta}, \quad B = -\frac{\lambda^2}{2ac}, \quad \varphi = \frac{hlcos\beta}{\sin^2\beta}, \quad A = \frac{D}{10},$$

and $\tau = 10\sin^2 2\theta$

The value of E, D, C, B, and A are given by

$$\Sigma\alpha\sin^2\theta = E\Sigma\alpha^2 + D\Sigma\alpha\gamma + C\Sigma\alpha\delta + B\Sigma\alpha\varphi + A\Sigma\alpha\tau,$$

$$\Sigma\gamma\sin^2\theta = E\Sigma\alpha\gamma + D\Sigma\gamma^2 + C\Sigma\gamma\delta + B\Sigma\gamma\varphi + A\Sigma\gamma\tau,$$

$$\Sigma\delta\sin^2\theta = E\Sigma\alpha\delta + D\Sigma\gamma\delta + C\Sigma\delta^2 + B\Sigma\delta\varphi + A\Sigma\delta\tau,$$

$$\Sigma\varphi\sin^2\theta = E\Sigma\alpha\varphi + D\Sigma\gamma\varphi + C\Sigma\delta\varphi + B\Sigma\varphi^2 + A\Sigma\varphi\tau,$$

$$\Sigma\tau\sin^2\theta = E\Sigma\alpha\tau + D\Sigma\gamma\tau + C\Sigma\delta\tau + B\Sigma\varphi\tau + A\Sigma\tau^2.$$

3. Results and Discussion

$LiTaO_3$ thin films were characterized at annealing process of 800 ^oC for 1, 8, 15, and 22 hours. According to the XRD data, can be seen several peaks which were correspond to Si (100), SiO_2 (040; 030), $LiTaO_3$ and $LiTaSiO_5$, where the dominance phases were Si and $LiTaSiO_5$ [17,18]. $LiTaSiO_5$ was formed from reaction between $LiTaO_3$ and silicon substrates which occured due to its annealing temperature (800 ^oC) which was higher than literature (600 ^oC) [19]. Spin coating at a speed of 500 rpm and polymeric organic solution method (Pechini method) with annealing temperature of 600 ^oC for 3 hours acquired $LiTaO_3$ peaks at hkl (012), (104), (110), (006), (202), (024), (116), (122), (018), (214), (300) [19]. Annealing temperature of 800 ^oC will cause enhancement of thermal vibration energy which was responsible for the phase transformation of $LiTaO_3$ into $LiTaSiO_5$. Figure 1 shows the XRD pattern of $LiTaSiO_5$ thin films after annealing temperature of 800 ^oC for 1, 8, 15, and 22 hours. There were peak intensity differences that formed on each graphic.

Heat treatment affected the nano scale grain size films which leads to denser, more compact, and more homogenous films. In monocrystallite orientation, the quality degree of crystallite was determined by high peak intensity. The higher intensity films leads to the better crystallite quality. The crystallite structures have sharp peak due to their long range order. On the contrary, the amorf structures have slightly slope peak due to their short range order. Film layer crystallity is proportional to the grain size. This means that the bigger grain size from film morphology, the better crystallite quality. Heat treatment also affected the material microstructures. The higher annealing temperature leads to the larger grain size. Increasing in temperature can increase the thermal vibration energy for accelerating the atom diffusion in the grain which impact to the grain size. The nano scale grain size calculation was given in Fig 2.

According to Table 1, the annealing times did not affect the lattice parameter, however, annealing times affected intensity and FWHM peaks. $LiTaSiO_5$ films have monoclinic crystallite structure within space group $P2_1/c$ (14) (JCPDS file 45-0644) (a = 7,514 Å, b = 7,929 Å, c = 7,445 Å) [47].

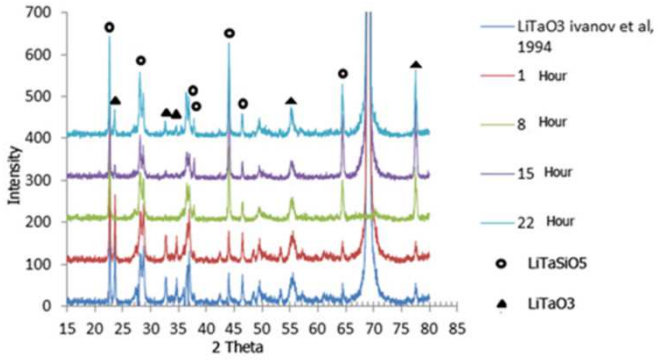

Fig 1. The XRD Pattern.

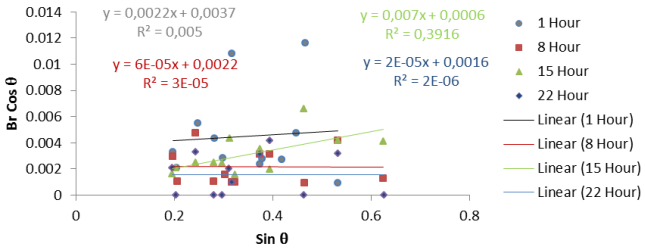

Fig 2. The Nano Scale Grain Size Calculation.

Table 1. *Lattice parameter of LiTaSiO5 after annealing process of 800°C (monoclinic).*

Lattice parameter	Annealing time (hour)				JCPDS Data [47]
	1	8	15	22	
a (Å)	6,2478	6,2478	6,2478	6,2478	7,5140
b (Å)	7,2785	7,2785	7,2785	7,2785	7,9290
c (Å)	6,1087	6,1087	6,1087	6,1087	7,4450

Nanoscale surface roughness of the films was calculated by section analysis of the height image [49]. The section analysis of the height image indicated increase in nanoscale roughness for films with additives. AFM phase image can be used to map stiffness difference on the surface. The effect of growth, annealing temperature and times of

$LiTaSiO_5$ on the surface morphology were carried out by using the AFM images [20-26]. Figure 3,4, and 5 show surface, nano scale grain size, three dimension analysis on 2000 nm x 2000 nm area at 800^oC. Those figures also show surface roughness, mean grain size, grain diameter with various annealing times [27-34]. The RMS surface roughness for $LiTaSiO_5$ thin films on 2000 nm x 2000 nm area at 800 ^oC for 1, 8, 15, and 22 hours were 4.989 nm, 10.7 nm, 9.684 nm, 50.73 nm, respectively, whereas the grain size (mean diameter) for 1, 8, 15, and 22 hours were 357.6 nm, 675.1 nm, 414.5 nm, and 214.7 nm, respectively. From Table 2, can be concluded that the AFM can show more detail data than the XRD [35-38]. Both of methods have several advantages, strain scores can be acquired from the XRD analysis, while RMS roughness and mean size scores can be acquired from the AFM analysis. Some information about the relative surface tensions of different crystal planes can be obtained by observing the relative development of various facets in field ion microscopy [39].

Table 2. *The results of the XRD and AFM analysis.*

Annealling Time (h)	XRD		AFM		
	Grain Size (nm)	Strain	Grain Size/ Mean Diameter (nm)	RMS Roughness (nm)	Mean Size (nm^2)
1	41.63700	0.00220	357.6	4.989	100400
8	70.02500	0.00006	675.1	10.7	358000
15	256.76000	0.00700	414.5	9.684	134900
22	96.28500	0.00002	214.7	50.73	36210

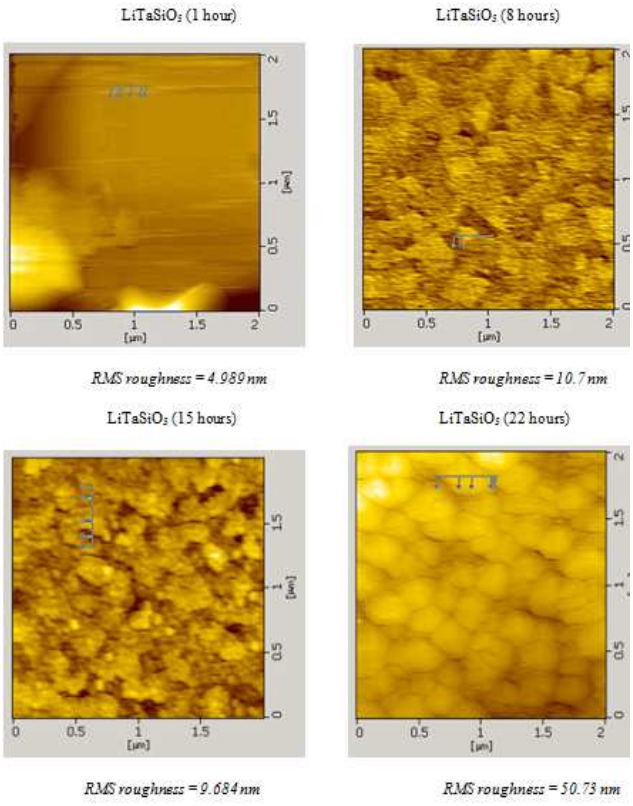

Fig 3. *Surface analysis using the AFM method at 800 °C of 2000 nm x 2000 nm area for $LiTaSiO_5$ thin films.*

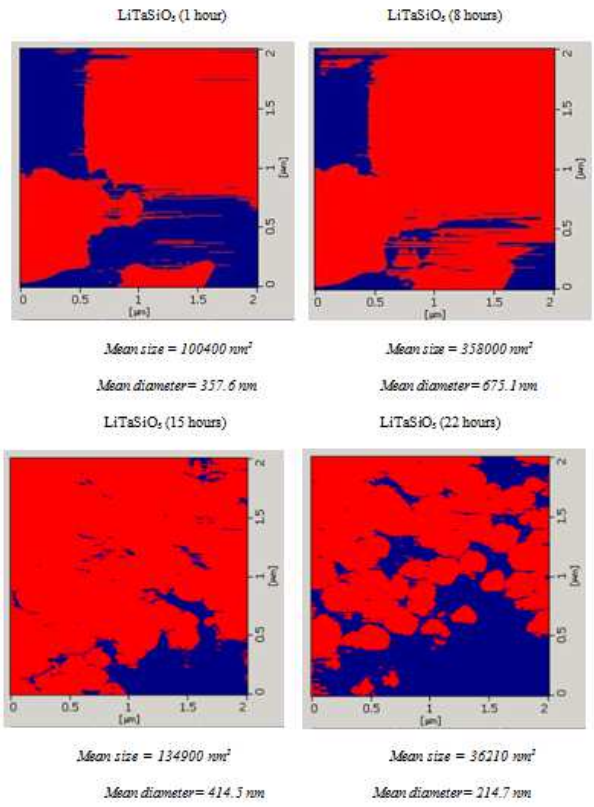

Fig 4. *Grain analysis using the AFM method at 800 °C of 2000 nm x 2000 nm area for $LiTaSiO_5$ thin films.*

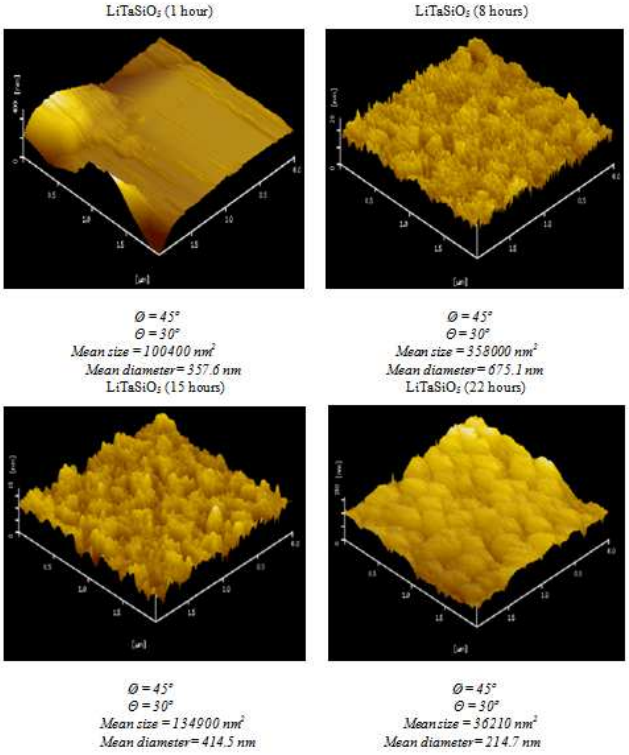

Fig 5. *Three dimension analysis using the AFM method at 800 °C of 2000 nm x 2000 nm area for $LiTaSiO_5$ thin films.*

The band gap energy, which is the separation between the energy of the lowest conduction band and that of the highest valance band [48], can be found by extrapolating $(\alpha hv)^{1/2}$ to 0 (*Tauc plot* method). The vertical and horizontal axis represent hv and $(\alpha hv)^{1/2}$, respectively, where α is absorbance coefficient (cm^{-1}). The optical absorbance coefficient α (E) was obtained from reflectance spectrum [24] of film thickness using volumetric method.

At the previously, the band gap energies of $LiTaSiO_5$ thin films were in the range of 1.3-3.5 eV [40,41], while the band gap energies in this research were around 2.62-3.43 eV as shown in Table 3. These ranges can be caused by annealing times, solid cystallite structure, surface roughness, and interatomic space of $LiTaSiO_5$. By comparing band gap energies of $LiTaSiO_5$ and semiconductor material (1-6 eV) [42-46], can be concloded that $LiTaSiO_5$ films in this research have semiconductor property.

Table 3. *Band gap energy of $LiTaSiO_5$ thin films.*

Number	Film sample		Band gap Energy (eV)
	Temp (°C)	Time (hour)	
1	800	1	2.62
2		8	3.43
3		15	2.71
4		22	3.10

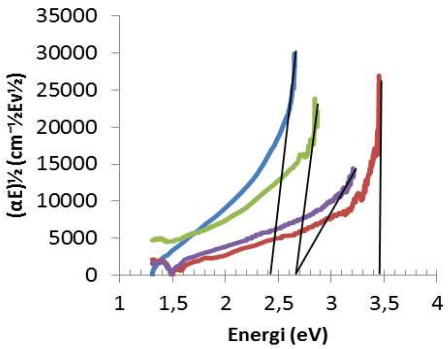

Fig 6. *Band gap of LiTaSiO5.*

4. Conclusions

The annealing process of 800 oC could affected LiTaSiO5 thin films structure (monoclinic structure). Nano scale grain size of LitaSiO5 can be calculated using the XRD and AFM. The XRD and AFM gave different results on nano scale grain size. Both of methods have several advantages, strain scores can be acquired from the XRD, while RMS roughness and mean size scores can be acquired from the AFM. Band gap can be calculated using Tauc plot method. The band gap energies were in the range of 2.62-3.43 eV which means that LiTaSiO5 thin films have semiconductor property (1-6 eV). Therefore, this material can be developed as infrared and colour sensors.

Acknowledgements

This work was supported by Incentive Grant of SINAS KMNRT, The Republic of Indonesia under contract No. 38/SEK/INSINAS/PPK/I/2013, and National Strategic Research of Directorate General of Higher Education, Ministry of National education, The Republic of Indonesia under contract no. 134/SP2H/PL/Dit.Litabmas/V/2013.

References

[1] Kostritskii S. M. et al. Quantitative evaluation of the electro-optic effect and second-order optical nonlinearity of lithium tantalate crystals of different compositions using Raman and infrared spectroscopy. Applied Physics B. 2005. doi: 10.1007/s00340-005-2046-4.

[2] Indro M N, Irzaman, Sastri B, Nady L, Syafutra H, Siswadi. Electric and Pyroelectric Properties of LiTaO3 and LiTaFe2O3. The International Conference on Materials Science and Technology. 1 (1) (2010), 303-308.

[3] Yan Tao et al. Formation mechanism of black LiTaO3 single crystals through chemical reduction. J. Appl. Cryst. 44 (2011), 158–162.

[4] Fang S, Wang B, Zhang T, Ling F and Wang R. Growth and photorefractive properties of Zn, Fe double-doped LiTaO3 crystal. Optical Materials. 28 (2006), 207-211.

[5] B.A. Baumert, L.H. Chang, A.T. Matsuda and C.J. Tracy. A Study of BST Thin Films for Use in bypass Capacitors. J. Mater. Res. 13 (1998), (1): 197.

[6] F. Wang, A. Uusimaki, S. Leppavuori, S.F. Karmanenko, A.I. Dedyk, V.I. Sakharov, I.T. Serenkov. BST Ferroelectric Film Prepared with Sol-Gel Process and Its Dielectric Performance in Planar Capacitor Structure. J. Mater. Res. 13 (1998), (5): 1243.

[7] M.A. Itskovsky. Kinetics of Ferroelectric Phase Transition : Nonlinear Pyroelectric Effect and Ferroelectric Solar Cell. Jpn. J. Appl. Phys. 38 (1999), (8): 4812.

[8] Irzaman, Darmasetiawan H, Hardhienata H, Erviansyah R, Akhiruddin, Hikam M, Arifin P. Electrical Properties of Photodiode BST Thin Film Doped with Ferrium Oxide using Chemical Deposition Solution Method. Journal Atom Indonesia, Batan. 6 (2010), (2): 57-62.

[9] E.S. Choi, J.C. Lee, J.S. Hwang, S.G. Yoon. Electrical Characteristics of The Contour Vibration Mode Piezoelectric Transformer with Ring/Dot Electrode Area Ratio. Jpn. J. Appl. Phys. 38 (1999), (9B): 5317.

[10] S. Momose, T. Nakamura, K. Tachibana. Effects of Gas Phase Thermal Decompositions of Chemical Vapor Deposition Source Moleculeson The Deposition of BST Films. Jpn. J. Appl. Phys. 39 (2000), (9B): 5384.

[11] M. Izuha, K. Ade, M. Koike, S. Takeno, N. Fukushima. Electrical Properties and Microstructure of Pt/BST/SrRuO3 Capacitors. Appl. Phys. Lett. 70 (1997), (11): 1405.

[12] J.S. Lee, J.S. Park, J.S. Kim, J.H. Lee, Y.H. Lee, S.R. Hahn. Preparation of BST Thin Films with High Pyroelectric Coefficients an Ambient Temperatures. Jpn. J. Appl. Phys. 38 (1999), (5B): L574.

[13] S. Kim, T.S. Kang, J.H. Je. Structural Characterization of Laser Alblation Epitaxial BST Thin Films on MgO (001) by Synchrotron x-Ray Scattering. J. Mater. Res. 14 (1999), (7): 2905.

[14] Irzaman, Maddu A, Syafutra H and Ismangil A. Uji konduktivitas listrik dan dielektrik film tipis lithium tantalate (LiTaO3) yang didadah niobium pentaoksida (Nb2O5) menggunakan metode chemical solution deposition. Di dalam: prosiding seminar nasional fisika. hlm 175-183. 2010. (In Indonesia)

[15] I. Ratera, J. Chen1, A Murphy, D.F. Ogletree1, J.M.J. Fr´echet and M. Salmeron. Atomic force microscopy nanotribology study of oligothiophene self-assembled films. Nanotechnology. 16 (2005), S235.

[16] P.D. Sawant and D V Nicolau. Hierarchy of DNA immobilization and hybridization on poly-L- lysine: an atomic force microscopy study. I Institute of Physics Publishing Smart Materials and Structures. Smart Mater. Struct. 15 (2006), S99–S103.

[17] B.D. Cullity. Element of X-RAY DIFFRACTION second edition. London: addison-wesley publishing company, INC. 1978.

[18] Suryanarayana C and Norton M G. X-Ray Diffraction A Practical Approach. New York: Plenum Press. 1998.

[19] Gonzalez A H M, Simoes A Z, Zaghete M A and Varela J A. Effect of preannealing on the morphology of LiTaO3 thin films prepared from the polymeric precursor method. Materials Characterization. 50 (2003), 233-238.

[20] Tagami Y, Ikigai H, Oishi Y. AFM observations of (DMPC/cholesterol) mixed monolayer on aqueous solution of Vibrio cholerae hemolysin. Colloids and Surfaces A: Physicochem. Eng. Aspects. (2006), 284–285. 475–479.

[21] Pang C L, Ashworth T V, Raza H, Haycock S A, Thornton G. A non-contact atomic force microscopy and 'force spectroscopy' study of charging on oxide surfaces. Nanotechnology 15 (2004), 862–866.

[22] Guilfoyleyx S J, Chewyk A, Moiseiwitschz N E, Sykesyk D E, Pettyyk M. Atomic force microscopy investigation of polysilicon films before and after SIMS analysis: the effects of sample rotation. J. Phys: Condens. Matter. 10 (1998), 1699–1706.

[23] Feng W, Ding Y, Liu Y, Lu R. The photochromic process of polyoxometalate-based nanocomposite thin film by in situ AFM and spectroscopy. Materials Chemistry and Physics. 98 (2006), 347–352.

[24] Lobo R F M, Pereira-da-Silva M A, Raposo M, Faria R. M, and Jr O N Oliveira. The morphology of layer-by-layer films of polymer/polyelectrolyte studied by atomic force microscopy. Nanotechnology. 14 (2003), 101–108.

[25] Mazher J, Shrivastav A K, Nandedkar R V and Pandey R K. Strained ZnSe nanostructures investigated by x-ray diffraction, atomic force microscopy, transmission electron microscopy and optical absorption and luminescence spectroscopy. Nanotechnology. 15 (2004), 572–580.

[26] Hishida M, Seto H, Kaewsaiha P, Matsuoka H, dan Yoshikawa K. Stacking structures of dry phospholipid films on a solid substrate. Colloids and Surfaces A: Physicochem. Eng. Aspects. (2006), 284–285;444–447.

[27] Stark R W. Spectroscopy of higher harmonics in dynamic atomic force microscopy. Nanotechnology 15 (2004), 347–351.

[28] H Ju-Hung, H Ming-Hung, L Hsiao-Hsien and L Heh-Nan. Selective growth of silica nanowires on nickel nanostructures created by atomic force microscopy nanomachining. Nanotechnology. 17 (2006), 170–173.

[29] Porti M, Nafr´ıa M, Aymerich X, Olbrich A and Ebersberger B. Post-breakdown electrical characterization of ultrathin SiO2 films with conductive atomic force microscopy. Nanotechnology. 13 (2002), 388–391.

[30] Miyake S and Kim J. Nanoprocessing of silicon by mechanochemical reaction using atomic force microscopy and additional potassium hydroxide solution etching. Nanotechnology. 16 (2005), 149–157.

[31] Sun Y and Pang John H L. AFM image reconstruction for deformation measurements by digital image correlation. Nanotechnology. 17 (2006), 933–939.

[32] Trevethan T and Kantorovich L. Models of atomic scale contrast in dissipation images of binary ionic surfaces in non-contact atomic force microscopy. Nanotechnology. 17 (2006), S205–S212.

[33] Sushko M L, Gal A Y, Watkins M and Shluger A L. Modelling of non-contact atomic force microscopy imaging of individual molecules on oxide surfaces. Nanotechnology. 17 (2006), 2062–2072

[34] Ryan P J, Adams G G, McGruer N E, and Muftu S. Contact scanning mode AFM for nanomechanical testing of free-

standing structures. J. Micromech. Microeng. 16 (2006), 1040–1046.

[35] Irzaman, Marwan A. Arief A, Hamdani R A, Komaro M. Electrical Conductivity and Surface Roughness Properties of Ferroelectric Gallium Doped BST Thin Film. Indonesian Journal of Physics, Departemen of Physics FMIPA ITB. (2008), 119-121.

[36] Irzaman, Darmasetiawan H, Hardhienata H, Hikam M, Arifin P, Jusoh S N, Taking S, Jamal Z, Idris M A. Surface Roughness and Grain Size Characterization of Effect of Annealing Temperature for Growth Gallium and Tantalum Doped Ba0.5Sr0.5TiO3 Thin Film. Journal Atom Indonesia, Batan. 35 (2009), (1): 57-67.

[37] Irzaman, Barmawi M, Crystallography and Surface Morphology of Ta2O5 Doped PZT Thin Film. Jurnal Sains MIPA, FMIPA Universitas Lampung. 13 (2007), (2): 84-88.

[38] Irzaman, Jamal Z, Idris M S, Kurnia D, Barmawi M. Microstrain, Particle Size and Lattice Constant of CaCO3 Ceramic by Rietveld Analysis. An International Publication of The Malaysia Nuclear Society (MNS). 4 (2007), (1): 43-46.

[39] Adamson A R. Physical Chemistry of Surfaces Fourth Edition. California: John Wiley & Sons, Inc. 1982.

[40] Youssef S, Al Amar R, Podlecki J, Sorli B and Foucaran A. Structural and optical characterization of oriented LiTaO3 thin films deposited by sol-gel technique [abstract]. Eur. Phys. J. Appl. Phys. 43 (2008), (1): 65-71.

[41] Cabuk S and Mamedov A. A Study of the LiNbO3 and LiTaO3 Absorption Edge. Tr. J. of Physics. 22 (1998), 41-45.

[42] Muktavat K and Upadhayaya A K. Applied Physics. New Delhi: L.K. International publishing House Pvt. Ltd. 2010.

[43] Irzaman, Syafutra H, Rancasa E, Nuayi A W, Rahman T G N, Nuzulia N A, Supu I, Sugianto, Tumimomor F, Surianty, Muzikarno O, Masrur. The Effect of Ba/Sr ration Electrical and Optical Properties of BaxSr(1-x)TiO3 (x= 0.25; 0.35; 0.45; 0.55) Thin Film Semiconductor. Ferreoelectrics. (2013), 445 (1), 4 – 17.

[44] Darmasetiawan H, Irzaman, Indro M N, Sukaryo S G, Hikam M, Bo N P. Optical Properties of Crystalline Ta2O5 Thin Films. Physica Status Solidi (a), Germany. 193 (2002), (1), 53-60.

[45] Irzaman, Darvina Y, Fuad A, Arifin P, Budiman M, Barmawi M. Physical and Pyroelectric Properties of Tantalum Oxide Doped Lead Zirconiuum Titanate [Pb0.9950(Zr0.525Ti0.465Ta0.010)O3] Thin Films and Its Application for IR Sensor. Physica Status Solidi (a), Germany. 199 (2003), (3): 416-424.

[46] Raksa Y T, Hikam M, Irzaman. Rietveld Analysis of Ferroelectric Pb Zr0.525Ti0.475O3 Thin Films. Ceramics International. 30 (2004), 1483-1485.

[47] Ivanov S, Zhurov V and Karpov Inst. 1994. Of Physical Chemistry, Moscow, Russia, ICDD Grant-in-Aid (JCPDS file 45-0644).

[48] Sze, S M. Physics of Semiconductor Devices. New Jersey : John Wiley & Sons, Inc. 1981.

[49] Hedge R, GS Bhat, B Deshpande. Morphology and properties of nylon 6 blown films reinforced with different weight percentage of nanoclay additives, International Journal of Polymer Science, 2012.